Research Article

Journal of Applied Toxicology

Received: 9 November 2014, Revised: 30 April 2015, Accepted: 5 May 2015 Published online in Wiley Online Library: 23 June 2015

(wileyonlinelibrary.com) DOI 10.1002/jat.3187

Accumulation and toxicity of intravenously-injected functionalized graphene oxide in mice

Kai-Ping Wen[a], Ying-Chieh Chen[b]*, Chia-Hui Chuang[b], Hwan-You Chang[c], Chi-Young Lee[a] and Nyan-Hwa Tai[a]*

ABSTRACT: Graphene and its functionalized derivatives have recently emerged as interesting nanomaterials with promising applications in biomedicine. In this study, the long-term *in vivo* biodistribution of intravenously injected nanographene oxide (NGO) functionalized with poly sodium 4-styrenesulfonate (PSS) was systematically examined and the potential toxicity over 6 months of NGO-PSS nanoparticles was investigated. Our results showed that the nanoparticles mainly accumulate in the lung, liver and spleen, where they persist for at least 6 months. These nanoparticles result in acute liver injury and chronic inflammation of the lung, liver and spleen, as evidenced by blood biochemistry results and histological examinations.

Additional supporting information may be found in the online version of this article at the publisher's web-site.

Keywords: graphene oxide; intravenous injection; biodistribution; toxicology

Introduction

Owing to its fascinating physical and chemical properties (Partoens and Peeters, 2006; Frank *et al*., 2007; Balandin *et al*., 2008; Chen *et al*., 2008; Lee *et al*., 2008; Nair *et al*., 2008;), graphene has attracted tremendous attention and has been widely applied in various fields, including quantum physics, nanoelectronic devices, energy research, transparent conductors, nanocomposite materials and catalysts (Huang *et al*., 2012; Loh *et al*., 2010; Stankovich *et al*., 2006). With its two-dimensional (2D) planar structure, nanoscale graphene provides an ultra-high surface area for efficient molecular loading and bioconjunction. Because of this special property, nanoscale grapheme, with appropriate surface functionalization, can be used for drug and gene delivery (Feng *et al*., 2011; Liu, Davis, *et al*., 2008; Tian *et al*., 2011; Yang *et al*., 2011; Zhang *et al*., 2010) and in biosensors (Akhavan *et al*., 2012; He *et al*., 2010; Tang *et al*., 2010; Wen *et al*., 2012). Owing to its intrinsic high near-infrared absorbance and fluorescence, functionalized graphene and its nanocomposites have also been used as photothermal agents for cancer treatment and as contrast agents for bioimaging (Hong *et al*., 2012; Robinson *et al*., 2011; Sun *et al*., 2008; Yang *et al*., 2010, Yang *et al*., 2012; Zhang *et al*., 2012). In addition, graphene-based materials have recently been used, with encouraging outcomes, as scaffolds for controlling cell growth and differentiation (Chen *et al*., 2012; Lee *et al*., 2011; Li *et al*., 2011; Nayak *et al*., 2011).

Due to the extensive use of graphene-related materials and the growing interest in applying them on a large scale in industry, the potential exposure risk and toxicity of graphene have become a major concern. However, safety considerations of the use of these complex materials have not been satisfactorily explored and there are no clear conclusions on toxicity (Wang *et al*., 2011; Zhang, Yang, *et al*., 2011) and, thus, there is an urgent need for a clear understanding of the safety profile of graphene and its effects on humans. In this study, we intensively investigated the biodistribution and toxicity of nanographene oxide–poly sodium 4-styrenesulfonate (NGO-PSS) after intravenous (i.v.) injection into healthy mice using an *in vivo* imaging system (IVIS), histological examination and analysis of serum biochemical parameters.

Materials and Methods

Synthesis and Characterization of Nanographene Oxide

Pristine graphite rods (purity = 6 N) were purchased from Central Carbon Co Ltd, Taiwan. PSS was purchased from Sigma-Aldrich (St. Louis, MO, USA) and used without further purification. NGO-PSS nanoparticles were synthesized by a published one-step electrochemical exfoliation method (Su *et al*., 2011; Wang *et al*., 2009) with minor modifications. PSS powder (7 g) was dissolved in 100 ml of distilled water, two graphite rods were immersed in it to act as electrodes, and electrolysis was performed at a voltage of 5 V for 24 h, forming a suspension of NGO-PSS particles that was then ultrasonicated for 24 h. The resulting suspension was then sequentially filtered on 3-μm, 1-μm and 220-nm filters to obtain particles with sizes between 220 nm and 1 μm. The purified

*Correspondence to: Ying-Chieh Chen, National Hsinchu University of Education, Department of Applied Science, Hsinchu City, Taiwan 30014.
E-mail: yingchiehchen@gmail.com

Nyan-Hwa Tai, National Tsing Hua University, Department of Materials Science and Engineering, Hsinchu City, Taiwan 30013.
E-mail: nhtai@mx.nthu.edu.tw

[a]National Tsing Hua University, Department of Materials Science and Engineering, Hsinchu City, Taiwan 30013

[b]National Hsinchu University of Education, Department of Applied Science, Hsinchu City, Taiwan 30014

[c]National Tsing Hua University, Department of Life Science, Hsinchu City, Taiwan 30013

NGO-PSS nanoparticles were characterized by Raman spectroscopy (LabRam HR-800), Fourier transform-infrared spectroscopy (FT-IR) (Perkin-Elmer Spectrum RX), atomic force microscopy (AFM) (Bruker), and size distribution and surface zeta-potential analysis (Malvern Zeta Nanosizer).

Animal Housing, Injection and Sample Collection

The purified NGO-PSS nanoparticles were suspended in phosphate-buffered saline (PBS) at concentrations of 0.5, 1.0 and 2.0 mg ml^{-1} under sterile conditions. All animal experiments were performed in compliance with institutional ethics committee regulations and guidelines on animal welfare (Animal Care and Use Program Guidelines of National Tsing Hua University).

Male Balb/c mice (~25 g) were obtained from Bio-LASCO, Taiwan. In a short-term distribution experiment, one mouse was left untreated, and another injected i.v. with 3.2 mg kg^{-1} (0.2 ml) NGO-PSS nanoparticles labeled with the fluorescent dye Cy7 (see below). In the main study, four groups of five mice were housed in plastic cages and kept on a 12-h light/dark cycle, with food and water provided *ad libitum*. After acclimation for a week, the five mice in the same cage were injected i.v. (tail vein) with 0.2 ml of either one of the above NGO-PSS suspensions (equivalent to 4, 8, and 16 mg kg^{-1}) or PBS (control group). On days 1, 28, 90 and 180, mice from each group were sacrificed for distribution studies and histopathological examination by a toxicologic pathologist, Liang Chung-Tiang, DVM/Ph.D., associate scientist in National Laboratory Animal Center, Taiwan. Before sacrifice, blood samples were taken from all remaining mice on days 1, 7, 14, 28, 90 and 180, and body weight and behavior were recorded.

Biodistribution

In a study on the short-term distribution of NGO-PSS nanoparticles in mice after injection, NGO-PSS nanoparticles were labeled with the near-IR fluorescence dye Cy7 using a published method (Yang *et al.*, 2010) and injected i.v. (0.2 ml; dose 3.2 mg kg^{-1}) into one mouse, while another mouse was left untreated, then an *in vivo* and *in situ* imaging system (IVIS) was used to acquire fluorescence images at 1 min, 30 min and 24 h post-injection (p.i.), then the mice were sacrificed at 24 h p.i. and spectral imaging of the major organs was performed using IVIS. The long-term biodistribution was examined in the four groups of five mice injected with different doses of NGO-PSS nanoparticles or PBS described above by taking peritoneal images of one mouse from each group at days 1, 14, and 28.

Serum Biochemical Parameters

Blood samples were taken from the facial vein, and serum samples prepared by centrifugation of the clotted blood for 15 min at room temperature. All biochemical assays were performed using a clinical automatic chemistry analyzer (Hitachi 7080, Holliston,

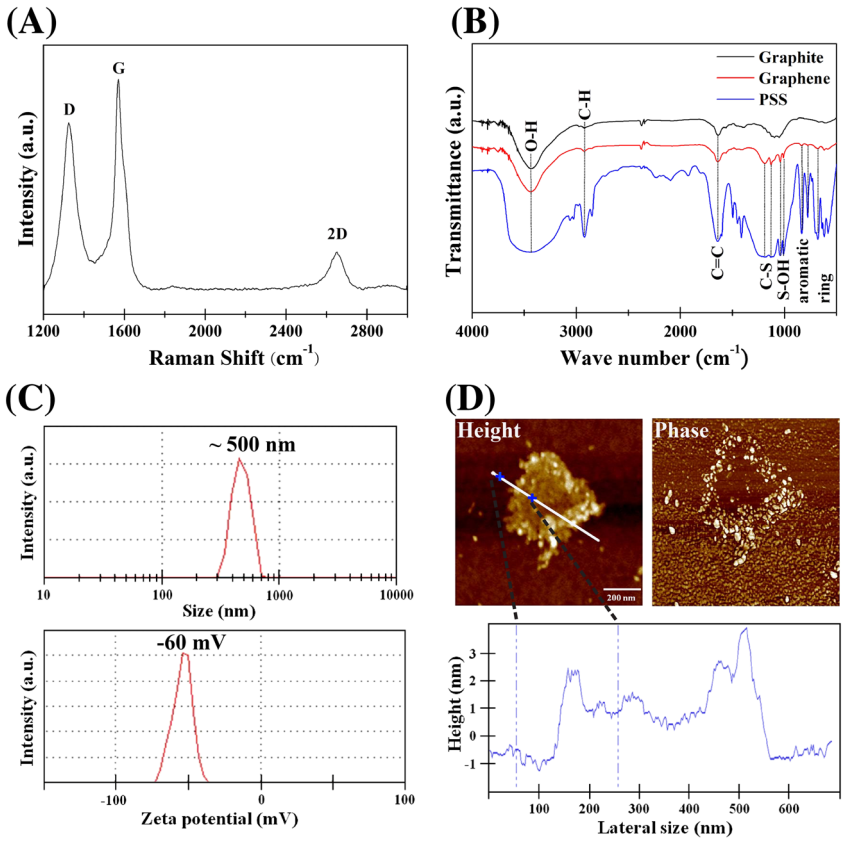

Figure 1. Characterization of nanographene oxide–poly sodium 4-styrenesulfonate (NGO-PSS) nanoparticles. (A) Raman spectrum of the NGO-PSS nanoparticles. (B) Fourier transform-infrared spectroscopy (FT-IR) spectra of graphite, PSS and NGO-PSS nanoparticles. (c) Zeta potential (top panel) and size distribution (bottom panel) of the NGO-PSS nanoparticles. (d) Atomic force microscopy (AFM) images; the blue lines indicate the thickness measured at the indicated points in the substrate and the center of the nanoparticle of the white line scan.

Journal of Applied Toxicology

MA,USA). The liver and kidney functional parameters examined were serum levels of aspartate transaminase (AST), alanine transaminase (ALT), alkaline phosphatase (ALP), blood urea nitrogen (BUN), creatinine (CREA), total protein (TP) and albumin (ALB).

Histological Observations and Immunohistochemical Analysis

One mouse from each group of the PBS or NGO-PSS nanoparticle-injected mice was sacrificed at 1, 28, 90 and 180 days p.i. and the heart, lung, liver, one kidney and the spleen collected for determination of accumulation and toxicological assays. The organs were fixed overnight in 10% neutral-buffered formalin and embedded in paraffin for analyses. The formalin-fixed tissue samples were thin-sectioned, mounted on glass microscope slides using standard histopathological techniques, stained with hematoxylin-eosin (H&E), and examined by light microscopy. For immunohistochemistry, 7-μ sections were deparaffinized, and antigen retrieval was carried out by heating the sections in 2-amino-2-hydroxymethyl-propane-1,3-diol (Tris)-EDTA buffer [10 mM Tris-Base, 2 mM EDTA, 0.05 % polyoxyethylene sorbitan monolaurate (Tween-20), pH 8.0]. The sections were blocked for 30 min in blocking serum (5%) and incubated with mouse-specific CD68 monoclonal antibody (1:25; GeneTex) for 1 h at room temperature. Secondary antibody incubations were carried out for 1 h at room temperature using FITC-conjugated secondary antibodies (1:100; Millipore). All of the fluorescently stained sections were counterstained with DAPI (Invitrogen).

Results

Characterization of Nanographene Oxide

To obtain a well-dispersed graphene suspension, we used a slightly modified published electrochemical exfoliation method (Su *et al*., 2011; Wang *et al*., 2009) to synthesize and functionalize NGO. PSS was bonded onto NGO during the oxidation process of electrolysis to improve the hydrophilicity of NGO and prevent the re-stacking of NGO-PSS nanoparticles as a result of strong van der Waals interactions.

The NGO-PSS nanoparticles showed the characteristic 2D band of graphitic material in the Raman spectrum. The D band showed that defects primarily resulting from oxidation in the electrochemical reaction were present, but was lower than the G band, contributed by perfectly stacked carbon atoms, showing that the majority of the structures had a perfect lattice of carbon atoms (Fig. 1A). Successful functionalization of NGO with PSS and the high stability of the NGO-PSS nanoparticles in aqueous solution were evidenced, respectively, by the FTIR spectrum (Fig. 1B) and the negative zeta potential (–60 mV) (Fig. 1C, top panel), the latter showing good to excellent stability of the nanoparticles (Greenwood and Kendall, 1999; Hanaor *et al*., 2012). The Zetasizer distribution revealed that the average sheet diameter (assuming a round shape) of the NGO-PSS nanoparticles ranged from 300 to 700 nm (Fig. 1C, bottom panel), while AFM imaging showed that the nanoparticles formed island-like sheets with a lateral size of about 500 nm and a thickness of about 2 nm (Fig. 1D, left panel). In the AFM phase image (Fig. 1D, right panel), white spots were seen mainly on the margin of the NGO, showing successful bonding of PSS to NGO. These data demonstrate that the NGO-PSS nanoparticles were successfully dispersed in aqueous solution.

Biodistribution

To examine the short-term distribution of the NGO-PSS nanoparticles *in vivo* after injection, they were labeled with the fluorescent dyeCy7. The upper panel in Fig. 2 shows IVIS fluorescence images of a non-injected control mouse (A) and a mouse injected with 3.2 mg kg^{-1} NGO-PSS-Cy7 nanoparticles at 1 min (B) and 30 min (c) p.i., and the results show that, at 30 min p.i., the nanoparticles

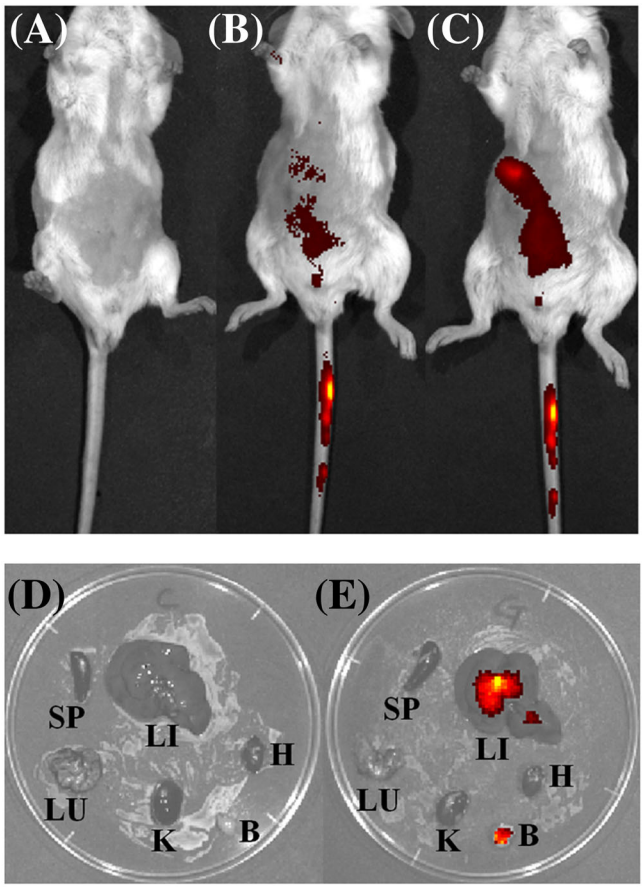

Figure 2. (A–C) *In vivo* imaging system (IVIS) fluorescence images of (A) a control mouse and (B and C) a mouse at (B) 1 min or (C) 30 min after injection of a dose of 3.2 mg kg^{-1} nanographene oxide–poly sodium 4-styrenesulfonate (NGO-PSS)-Cy7 nanoparticles. (D and E) Representative fluorescence images of different organs taken at 24 h post-injection (p.i.) from (D) the control mouse or (E) the NGO-PSS-Cy7 nanoparticle-injected mouse. SP: spleen, LU: lung, LI: liver, K: kidney, H: heart, B: bladder.

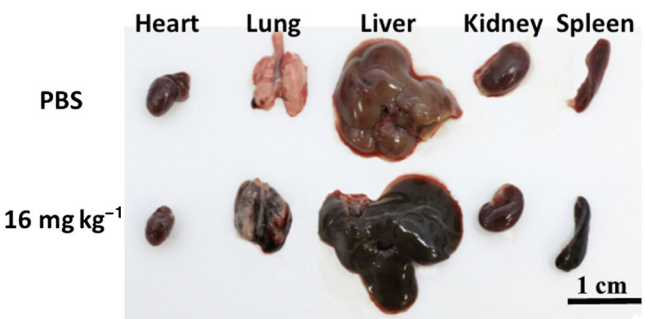

Figure 3. Images of major organs taken at day 14 from the control mouse (top row) or the mouse injected with 16 mg kg^{-1} nanographene oxide–poly sodium 4-styrenesulfonate (NGO-PSS).

were widely dispersed and tended to aggregate in the abdomen. At 24 h p.i., the intensity of the Cy7 fluorescence was rather low and spread throughout the whole body (data not shown.) To obtain a better understanding of the distribution of the NGO-PSS-Cy7 nanoparticles, two mice were sacrificed at 24 h p.i. and the organs collected and fluorescence images were taken; Fig. 2d shows the results for the control mouse and Fig. 2e those for the nanoparticle-injected mouse. No fluorescence was seen in the control organs, whereas the NGO-PSS-Cy7 nanoparticles were mainly distributed in the liver, with a little in the bladder. These data suggest that renal clearance might be involved in the excretion of NGO-PSS nanoparticles from the body.

We then studied the impact of i.v. injection of 4, 8 or 16 mg kg^{-1} NGO-PSS nanoparticles or PBS into four groups. Peritoneal images taken on day 1 showed that the color of the liver changed from dark red to black as the injection dose increased (data not shown),

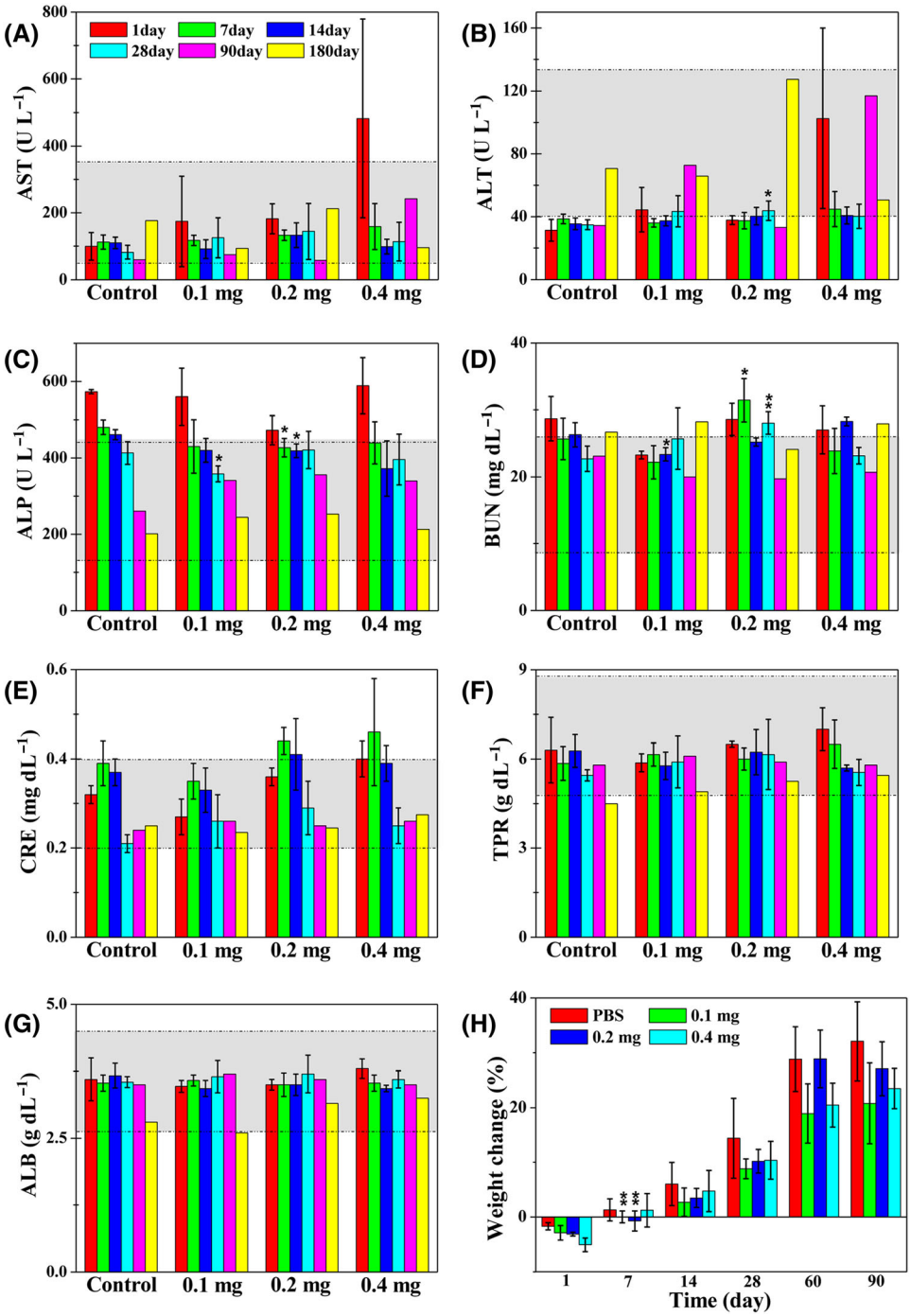

Figure 4. (A–G) Biochemical analysis of serum from male Balb/c mice injected with phosphate-buffered saline (PBS) or the different dosages of nanographene oxide–poly sodium 4-styrenesulfonate (NGO-PSS) nanoparticles taken on days 1, 7, 14, 28 and 90 post-injection (p.i.) (A) aspartate transaminase (AST), (B) alanine transaminase (ALT), (C) alkaline phosphatase (ALP), (D) blood urea nitrogen (BUN), (E) creatinine (CREA), (F) total protein (TP) and (G) albumin (ALB). The gray areas in the figures show the normal reference range for healthy male Balb/c mice. (H) Body weight time-course in the different groups (*$P < 0.05$, **$P < 0.01$).

Journal of Applied Toxicology

direct evidence for the uptake of the nanoparticles. At the highest dosage (16 mg kg^{-1}), the color of the liver turned from dark red (day 1) to black (day 14), then to brown (day 28) (data not shown). When the major organs in the mice injected with the high-dose NGO-PSS nanoparticles were compared at day 14 p.i. to those in the PBS-injected mouse, there were obvious differences in the color of the liver (Fig. 3), consistent with the IVIS biodistribution results (Fig. 2E). In mice injected with NGO-PSS nanoparticles, the color of the lung, liver and spleen changed from red to black, direct evidence for their uptake.

Serum Biochemical Parameters

To evaluate the toxicity of the NGO-PSS nanoparticles, serum biochemical parameters were measured in the four groups of mice on day 1, 7, 14, 28, 90 and 180. AST, ALT and ALP levels (important indicators of hepatic injury) showed a large increase on day 1 in the 16-mg kg^{-1} group (Fig. 4A, B), demonstrating that NGO-PSS nanoparticles induced acute hepatic injury. With the exception of ALT levels in the 16 mg kg^{-1}-treated mouse that were again elevated on day 90, although within the normal range, ALT and AST levels dropped back to the normal range at later time points (days 7–90), indicating that the injury caused by the NGO-PSS nanoparticles was reversible. ALP levels in all four groups exceeded the normal range on day 1, then fell back to the normal range (Fig. 4C). BUN, CRE, TPR and ALB levels (indicators of kidney function) were also in the normal range except for slight variations in BUN and CRE levels (Fig. 4D–G). Except for the high AST and ALT levels in the high dosage group on day 1 and the trend to higher ALT levels on day 90, all of the above parameters in the different NGO-PSS nanoparticle-treated groups at the different times p.i. were not significantly different from those in the control group and were within the reference normal ranges. Thus, no appreciable toxicity of NGO-PSS nanoparticles was noted in terms of biochemical parameters. In addition, the mice did not show differences in vocalization, labored breathing, difficulty in moving, hunching, or interactions with cage mates in any group. Except for day 1 p.i., body weight showed a gradual increase in all groups with time (Fig. 4H).

Histological Observations

To confirm the distribution and clearance of the NGO-PSS nanoparticles, the organs collected at days 1, 28, 90 and 180 p.i. were sliced, stained with H&E and examined for damage. At the doses of 8 and 16 mg kg^{-1}, but not 4 mg kg^{-1}, large numbers of black spots owing to accumulation of nanoparticles were in the lung at days 1, 28, 90 and 180 (Fig. 5, arrows) and in the liver at day 28, 90 and 180 (Fig. 6, arrows), whereas, in the spleen, black spots were seen at days 1, 28 and 90, but only at the dosage of 16 mg kg^{-1} (Fig. 7, arrows). In the liver and lung slices, the size of the black spots tended to increase with time after injection of the nanoparticles. However, it is worth mentioning that the black spots were difficult to see in the liver at day 1 at all doses. Similar black spots have been observed in the liver of mice injected with carbon nanotubes (Yang *et al.*, 2008). The characteristic lesions seen at the dose of 16 mg kg^{-1} on day 90 were macrophages in the lung (Fig. 5) and of Kupffer cells in the liver (Fig. 6) and macrophage infiltration in the spleen (Fig. 7). In order to compare the degree of histopathological lesion between groups, mean histopathological scores were used for further statistical analysis by dividing the sum of the score per grade of affected mice and the total number of examined mice (Supplementary information Fig. 2). In general, the lung and liver lesions were more severe, i,e. the degree of histopathological lesion (Shackelford *et al.*, 2002) is moderate, at the dose of 8 and 16 mg kg^{-1}, and decreased with decreasing dose, consistent with the serum biochemistry results indicating hepatic injury at day 1 and 90 p.i. Moreover, to confirm the degrees of acute and chronic inflammation caused by NGO-PSS, we stained all livers slices with CD68 antibodies, which is positive expressed on activated macrophages only. From the statistical summary, there is no significant increase with increasing concentration of

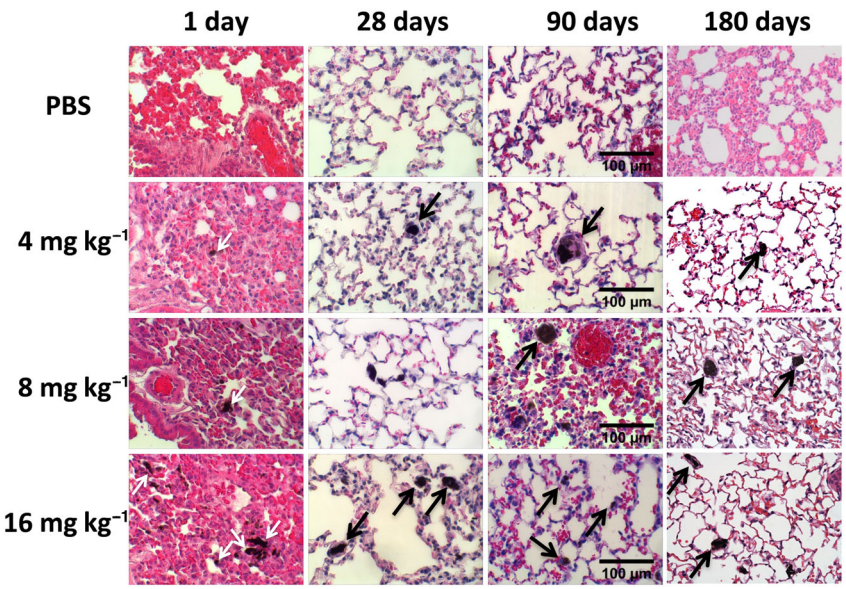

Figure 5. H&E-stained lung slices from the four groups of mice taken on days 1, 28, 90 and 180 post-injection (p.i.). Top to bottom: phosphate-buffered saline (PBS)-injected mouse and mice injected with 4, 8 or 16 mg kg^{-1} nanographene oxide–poly sodium 4-styrenesulfonate (NGO-PSS) nanoparticles (magnification: 400×; NGO-PSS aggregations: arrows).

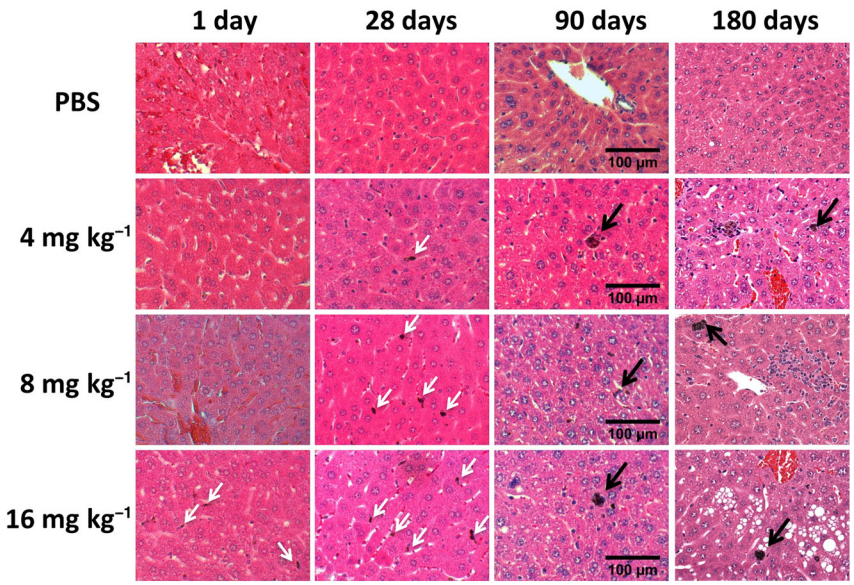

Figure 6. H&E-stained liver slices from the four groups of mice taken on days 1, 28, 90 and 180 post-injection (p.i.). Top to bottom: phosphate-buffered (PBS)-injected mouse and mice injected with 4, 8 or 16 mg kg^{-1} nanographene oxide–poly sodium 4-styrenesulfonate (NGO-PSS) nanoparticles (magnification: 400×; NGO-PSS aggregations: arrows).

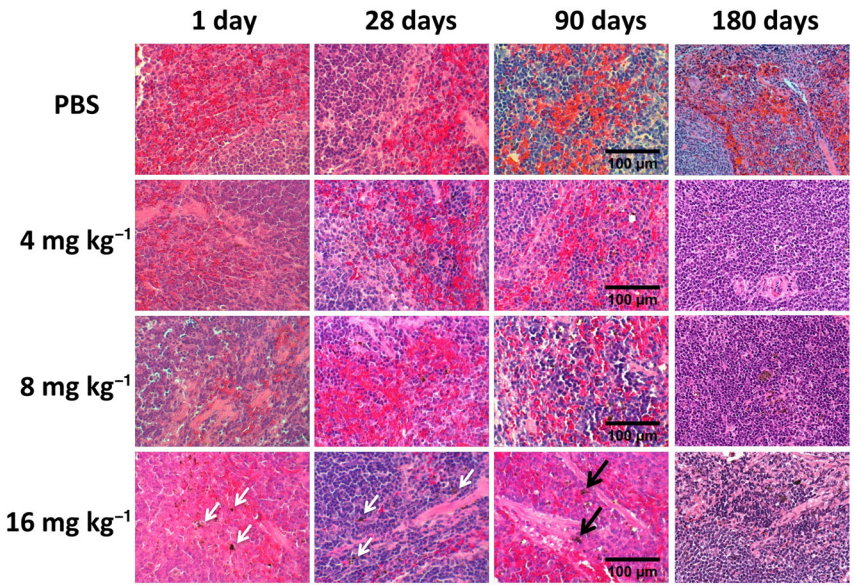

Figure 7. H&E-stained spleen slices from the 4 groups of mice taken on days 1, 28, 90 and 180 post-injection (p.i.). Top to bottom: phosphate-buffered saline (PBS)-injected mouse and mice injected with 4, 8 or 16 mg kg^{-1} nanographene oxide–poly sodium 4-styrenesulfonate (NGO-PSS) nanoparticles (magnification: 400×; NGO-PSS aggregations: arrows).

injected NGO-PSS, but decreasing with longer time points in all injected slices (Fig. 8). These results are consistent with our blood biochemical results.

Discussion

A number of groups have studied the *in vivo* behavior of functionalized NGO after i.v. injection and revealed the surface coating- and size-dependent biodistribution and toxicology profiles of this type of carbon-based nanomaterial. It has been reported in several previous studies (Wang *et al.*, 2011; Zhang, Yin, *et al.*, 2011), that pristine graphene or as-made graphene oxide (GO; lateral size $> 1\ \mu m$) injected i.v. into mice accumulates in the lung, resulting in pulmonary edema and granuloma formation. In contrast, surface-functionalized graphene and GO, with improved water dispersity and better stability in physiological environments, appear to be much less toxic (Singh *et al.*, 2012; Yang *et al.*, 2010). Other studies have shown that NGO functionalized with hydrophilic non-toxic polymers, such as polyethylene glycol or dextran, show no appreciable toxicity in mice for up to at least 3 months after i.v. injection at a high dose (20 mg kg^{-1}) (Yang *et al.*, 2010; Zhang, Yin, *et al.*, 2011). Unlike those GO-related materials with lateral sizes smaller than 20 nm Yang *et al.* (2010), those larger than 20 nm show high accumulation in the reticuloendothelial system (RES) of the mouse liver and spleen, which are responsible for the clearance of foreign materials by macrophage

Journal of Applied Toxicology

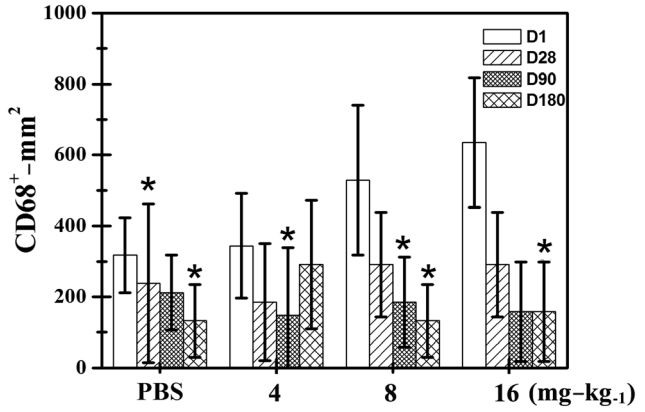

Figure 8. CD68 + -stained liver slices from the four groups of mice, including phosphate-buffered saline (PBS)-injected mouse and mice injected with 4, 8 or 16 mg kg^{-1} nanographene oxide–poly sodium 4-styrenesulfonate (NGO-PSS) nanoparticles, taken on days 1, 28, 90 and 180 post-injection (p.i.). (magnification: 400×).). *$P < 0.05$, compared with prior time points under the same dosage.

uptake (Yang *et al*., 2013). Interestingly, larger sized GO-related materials (>1 μm) show higher RES uptake than smaller sized NGO particles (<1 μm) (Yang *et al*., 2013), indicating that the size of the nanomaterial could also be an important factor regulating its body adsorption after i.v. injection.

Long-term accumulation seems to be a bio-property of most large-sized GO-related materials (Wang *et al*., 2011). Nano-GO particles (20 nm to 1 μm) (Yang *et al*., 2010, Yang *et al*., 2013) and GO particles (>1 μm) (Wang *et al*., 2011) are retained in the body for more than 1 month, whereas ultrasmall-sized GO (<20 nm) particles are not (Yang *et al*., 2010). In contrast to small-sized NGO particles, which are easily cleared by renal excretion (Yang *et al*., 2010), larger NGO particles accumulate in RES macrophages and are only excreted via the biliary pathway, although the process is very slow (Liu, Robinson, *et al*., 2008; Singh *et al*., 2012). All available data imply that the accumulation and long retention of NGO-PSS nanoparticles depend on their relatively large lateral size. The lateral size of NGO-PSS nanoparticles used in this study is around 500 nm (Fig. 1C). After injecting with varied concentration of NGO-PSS nanoparticles, it went to every organ in 30 min, stayed and accumulated as a function of concentration, especially in liver and bladder, shown in IVIS (Fig. 2). The black spots in the lung and liver were quite small at early time points at all doses of nanoparticles, but were larger at day 28 and day 90 (Fig. 5 and 6), and keep the size at day 180, which further confirming RES uptake of NGO-PSS nanoparticles after i.v. injection. Although the exact mechanism for body adsorption requires further investigation, it is likely that macrophages in RES organs gradually engulf i.v. injected NGO-PSS nanoparticles, consistent with the observation of liver color in Fig. 3. In H&E-stained spleen slices, we also noticed some brown-black pigments (Fig. 7), but these were relatively difficult to differentiate from the stained spleen cell nuclei. These findings suggest that studies on long-term toxicity are valuable and vital. Despite the long-term retention of NGO-PSS nanoparticles in RES organs and the high AST levels at day 1 p.i. shown in Fig. 4, they showed no appreciable toxicity in terms of blood chemistry and histology. The low toxicity of i.v. injected NGO-PSS nanoparticles might be due to an active protective mechanism, with RES uptake of nanoparticles post-injection. Our work is an important fundamental study that provides a deeper understanding of the *in vivo* behavior and toxicology of NGO-PSS nanoparticles in animals as a function of dosage.

Conclusions

We report the accumulation and toxicity in mice of i.v.-injected NGO-PSS nanoparticles. The majority of these nanoparticles accumulated in the abdominal area within a few minutes of injection and then gradually accumulated in the liver, lung, spleen and bladder. The only abnormalities in serum biochemical results were seen on day 1 in mice exposed to the high dosage of NGO-PSS (16 mg kg^{-1}), which caused acute liver toxicity. At 1 and 3 months (even 6 months) p.i., moderate chronic inflammation was detected in the liver and lung in mice given the dosage of 16 mg kg^{-1}. With increasing dosage of NGO-PSS nanoparticles, accumulation of black spots became more apparent and black spots were still detected in the lung and liver at 6 month p.i., demonstrating the long-term retention of NGO-PSS nanoparticles in the body. The results suggest that large size NGO-PSS nanoparticles cannot be used safely for biomedical applications. Further studies on the very important aspects of the clearance mechanism of NGO-PSS nanoparticles, especially the size effect of graphene sheets on their *in vivo* behaviors, are very important. More toxicological studies of this material at higher doses and using different animal models are necessary before graphene-related materials can be tested clinically.

Acknowledgments

This work was supported by the Ministry of Science and Technology (MOST), Taiwan under project numbers MOST 102-2221-E-134-001 and MOST 103-2221-E-134-001. The authors acknowledge the National Laboratory Animal Center, funded by the MOST of Taiwan, for technical support and histopathological examination in the histology-related experiments.

Conflict of Interest

The authors did not report any conflict of interest.

References

Reference ranges of biochemistry data of healthy female Balb/c mice were obtained from Charles River Laboratories: http://www.criver.com/files/pdfs/rms/balbc/rm_rm_r_balb-c_mouse_clinical_pathology_data.aspx.

Akhavan O, Ghaderi E, Rahighi R. 2012. Toward Single-DNA Electrochemical Biosensing by Graphene Nanowalls. *ACS Nano* **6**: 2904–2916.

Balandin AA, Ghosh S, Bao WZ, Calizo I, Teweldebrhan D, Miao F, Lau CN. 2008. Superior thermal conductivity of single-layer graphene. *Nano Lett.* **8**: 902–907.

Chen GY, Pang DW, Hwang SM, Tuan HY, Hu YC. 2012. A graphene-based platform for induced pluripotent stem cells culture and differentiation. *Biomaterials* **33**: 418–427.

Chen JH, Jang C, Xiao S, Ishigami M, Fuhrer MS. 2008. Intrinsic and extrinsic performance limits of graphene devices on SiO2. *Nat. Nanotechnol.* **3**: 206–209.

Feng L, Zhang S, Liu Z. 2011. Graphene based gene transfection. *Nanoscale* **3**: 1252–1257.

Frank IW, Tanenbaum DM, van der Zande AM, McEuen PL. 2007. Mechanical properties of suspended graphene sheets. *J. Vac. Sci. Technol., B. Microelectron. Nanometer. Struct.* **25**: 2558.

Greenwood R, Kendall K. 1999. Selection of Suitable Dispersants for Aqueous Suspensions of Zirconia and Titania Powders using Acoustophoresis. *J. Eur. Ceram. Soc.* **19**: 479–488.

Hanaor D, Michelazzi M, Leonelli C, Sorrell CC. 2012. The effects of carboxylic acids on the aqueous dispersion and electrophoretic deposition of ZrO2. *J. Eur. Ceram. Soc.* **32**: 235–244.

He S, Song B, Li D, Zhu C, Qi W, Wen Y, Wang L, Song S, Fang H, Fan C. 2010. A Graphene Nanoprobe for Rapid, Sensitive, and Multicolor Fluorescent DNA Analysis. *Adv. Funct. Mater.* **20**: 453–459.

Hong H, Zhang Y, Engle JW, Nayak TR, Theuer CP, Nickles RJ, Barnhart TE, Cai W. 2012. In vivo targeting and positron emission tomography imaging of tumor vasculature with (66)Ga-labeled nano-graphene. *Biomaterials* **33**: 4147–4156.

Huang X, Qi X, Boey F, Zhang H. 2012. Graphene-based composites. *Chem. Soc. Rev.* **41**: 666–686.

Lee C, Wei X, Kysar JW, Hone J. 2008. Measurement of the elastic properties and intrinsic strength of monolayer graphene. *Science* **321**: 385–388.

Lee WC, Lim C, Shi H, Tang LAL, Wang Y, Lim CT, Loh KP. 2011. Origin of Enhanced Stem Cell Growth and Differentiation on Graphene and Graphene Oxide. *ACS Nano* **5**: 7334–7341.

Li N, Zhang X, Song Q, Su R, Zhang Q, Kong T, Liu L, Jin G, Tang M, Cheng G. 2011. The promotion of neurite sprouting and outgrowth of mouse hippocampal cells in culture by graphene substrates. *Biomaterials* **32**: 9374–9382.

Liu Z, Davis C, Cai W, He L, Chen X, Dai H. 2008. Circulation and long-term fate of functionalized, biocompatible single-walled carbon nanotubes in mice probed by Raman spectroscopy. *Proc. Natl. Acad. Sci. U. S. A.* **105**: 1410–1415.

Liu Z, Robinson JT, Sun XM, Dai HJ. 2008. PEGylated nanographene oxide for delivery of water-insoluble cancer drugs. *J. Am. Chem. Soc.* **130**: 10876-+.

Loh KP, Bao QL, Eda G, Chhowalla M. 2010. Graphene oxide as a chemically tunable platform for optical applications. *Nat. Chem.* **2**: 1015–1024.

Nair RR, Blake P, Grigorenko AN, Novoselov KS, Booth TJ, Stauber T, Peres NM, Geim AK. 2008. Fine structure constant defines visual transparency of graphene. *Science* **320**: 1308.

Nayak TR, Andersen H, Makam VS, Khaw C, Bae S, Xu XF, Ee PLR, Ahn JH, Hong BH, Pastorin G, Ozyilmaz B. 2011. Graphene for Controlled and Accelerated Osteogenic Differentiation of Human Mesenchymal Stem Cells. *ACS Nano* **5**: 4670–4678.

Partoens B, Peeters F. 2006. From graphene to graphite: Electronic structure around the K point. *Phys. Rev. B.* **74**: 075404.

Robinson JT, Tabakman SM, Liang Y, Wang H, Casalongue HS, Vinh D, Dai H. 2011. Ultrasmall reduced graphene oxide with high near-infrared absorbance for photothermal therapy. *J. Am. Chem. Soc.* **133**: 6825–6831.

Shackelford C, Long G, Wolf J, Okerberg C, Herbert R. 2002. Qualitative and quantitative analysis of nonneoplastic lesions in toxicology studies. *Toxicol. Pathol.* **30**: 93–96.

Singh SK, Singh MK, Kulkarni PP, Sonkar VK, Grácio JJA, Dash D. 2012. Amine-Modified Graphene: Thrombo-Protective Safer Alternative to Graphene Oxide for Biomedical Applications. *ACS Nano* **6**: 2731–2740.

Stankovich S, Dikin DA, Dommett GH, Kohlhaas KM, Zimney EJ, Stach EA, Piner RD, Nguyen ST, Ruoff RS. 2006. Graphene-based composite materials. *Nature* **442**: 282–286.

Su CY, Lu AY, Xu Y, Chen FR, Khlobystov AN, Li LJ. 2011. High-Quality Thin Graphene Films from Fast Electrochemical Exfoliation. *ACS Nano* **5**: 2332–2339.

Sun X, Liu Z, Welsher K, Robinson JT, Goodwin A, Zaric S, Dai H. 2008. Nano-Graphene Oxide for Cellular Imaging and Drug Delivery. *Nano Res.* **1**: 203–212.

Tang LAL, Wang JZ, Loh KP. 2010. Graphene-Based SELDI Probe with Ultrahigh Extraction and Sensitivity for DNA Oligomer. *J. Am. Chem. Soc.* **132** 10976–10977.

Tian B, Wang C, Zhang S, Feng LZ, Liu Z. 2011. Photothermally Enhanced Photodynamic Therapy Delivered by Nano-Graphene Oxide. *ACS Nano* **5**: 7000–7009.

Wang G, Wang B, Park J, Wang Y, Sun B, Yao J. 2009. Highly efficient and large-scale synthesis of graphene by electrolytic exfoliation. *Carbon* **47**: 3242–3246.

Wang K, Ruan J, Song H, Zhang J, Wo Y, Guo S, Cui D. 2011. Biocompatibility of Graphene Oxide. Nanoscale Research Letters. **6**: 8.

Wen H, Dong C, Dong H, Shen A, Xia W, Cai X, Song Y, Li X, Li Y, Shi D. 2012. Engineered redox-responsive PEG detachment mechanism in PEGylated nano-graphene oxide for intracellular drug delivery. *Small* **8**: 760–769.

Yang K, Gong H, Shi X, Wan J, Zhang Y, Liu Z. 2013. In vivo biodistribution and toxicology of functionalized nano-graphene oxide in mice after oral and intraperitoneal administration. *Biomaterials* **34**: 2787–2795.

Yang K, Wan J, Zhang S, Tian B, Zhang Y, Liu Z. 2012. The influence of surface chemistry and size of nanoscale graphene oxide on photothermal therapy of cancer using ultra-low laser power. *Biomaterials* **33**: 2206–2214.

Yang K, Wan J, Zhang S, Zhang Y, Lee ST, Liu Z. 2010. In Vivo Pharmacokinetics, Long-Term Biodistribution, and Toxicology of PEGylated Graphene in Mice. *ACS Nano* **5**: 516–522.

Yang K, Zhang S, Zhang G, Sun X, Lee ST, Liu Z. 2010. Graphene in mice: ultrahigh in vivo tumor uptake and efficient photothermal therapy. *Nano Lett.* **10**: 3318–3323.

Yang ST, Wang X, Jia G, Gu Y, Wang T, Nie H, Ge C, Wang H, Liu Y. 2008. Long-term accumulation and low toxicity of single-walled carbon nanotubes in intravenously exposed mice. *Toxicol. Lett.* **181**: 182–189.

Yang X, Wang Y, Huang X, Ma Y, Huang Y, Yang R, Duan H, Chen Y. 2011. Multi-functionalized graphene oxide based anticancer drug-carrier with dual-targeting function and pH-sensitivity. *J. Mater. Chem.* **21**: 3448.

Zhang L, Xia J, Zhao Q, Liu L, Zhang Z. 2010. Functional graphene oxide as a nanocarrier for controlled loading and targeted delivery of mixed anticancer drugs. *Small* **6**: 537–544.

Zhang S, Yang K, Feng L, Liu Z. 2011. In vitro and in vivo behaviors of dextran functionalized graphene. *Carbon* **49**: 4040–4049.

Zhang X, Yin J, Peng C, Hu W, Zhu Z, Li W, Fan C, Huang Q. 2011. Distribution and biocompatibility studies of graphene oxide in mice after intravenous administration. *Carbon* **49**: 986–995.

Zhang Y, Nayak TR, Hong H, Cai W. 2012. Graphene: a versatile nanoplatform for biomedical applications. *Nanoscale* **4**: 3833–3842.

Supporting Information

Additional supporting information may be found in the online version of this article at the publisher's web-site.